






Strength evolution laws in curing of solvent-welded polymers

Tousif Ahmed , Bing Han , Michael Sulecki, Marigrace Ferrill , and Zubaer M. Hossain ^{*}
*Laboratory of Mechanics and Physics of Heterogeneous Materials, Department of Mechanical Engineering,
 University of Delaware, Delaware 19716, USA*

 (Received 8 December 2020; accepted 28 January 2021; published 15 February 2021)

This paper reports the scaling laws to describe the time-evolution behavior of solvent-mediated strength at the interface between two identical thermoplastic polymers below the glass-transition temperature. Our results suggest that the evolution scales as \sqrt{t} , where t is the curing time. It depends on the time evolution of interfacial stiffness and toughness, each of which scales as \sqrt{t} . Employing a combination of experiments and continuum scale simulations, we show that the evolution of strength, stiffness, and toughness is controlled by pure diffusion. It can therefore be treated as a Gaussian process. While the “saturation of strength,” which describes the transition of strength evolution into a steady state, does not strictly follow any power-law type behavior, a simple exponential law accurately characterizes both evolution and saturation of strength. This suggests that the longer timescale nonlinear processes (that are overdetermined by the power-law type scaling laws) diminish rapidly in approaching a steady state. Furthermore, the kinetics of the evolution processes is well captured by the dissolution of polymer particles. While dissolution involves a different timescale, it strongly correlates with the solvent-welding process upon normalization. The correlation highlights the equivalence of the dissolution and solvent-joining processes and offers an easier route to determining strength at arbitrary curing times. Additionally, the dissolution rate of polymer particles is shape dependent and governed by the surface-to-volume ratio.

DOI: [10.1103/PhysRevE.103.022502](https://doi.org/10.1103/PhysRevE.103.022502)

I. INTRODUCTION

Mechanics of joining at the interface between two identical or dissimilar polymer materials plays a critical role in defining the effective mechanical behavior of composites [1–9]. The majority of existing studies focus on the joining process at temperatures higher than the glass-transition temperature, T_g , whereat the molecular motion is governed by reptation, reorganization, and rotation of polymer chains [10,11]. Above T_g , polymer chains disconnect and reconnect across the interface to bind the two sides. The underlying mechanisms are driven by the thermal energy and do not require any assistance from resins or additional ingredients [12]. Diffusion governs the evolution of strength in the joining process [11–18]. Consequently, the evolution of the “critical energy release rate” or fracture toughness, which correlates linearly with the number of polymer chains crossing the interface, scales as $t^{1/2}$. Likewise, the evolution of strength scales as $t^{1/4}$ under the assumption that the time-dependent relationship between fracture toughness and strength is independent of the elastic modulus [11]. Nevertheless, no scaling law seems to exist for joining processes that take place below T_g requiring no assistance from heat.

For example, scaling laws describing the time evolution of strength in solvent welding [9,19] remain undeveloped. This type of joining takes place below T_g and is facilitated by structural or engineering adhesives for various applications in adhesive technology, the plumbing industry, and compos-

ites to join plastics and woods [9,19–23]. In this process, interpenetration of the polymeric materials and formation of physical links across the interface involve reactions between the solvent and the materials to be bonded. The solvent diffuses into the free volume of the material and causes the polymeric chains across the interface to relax. Subsequently, a gel forms at the solvent-polymer interface [24–32] and two such interfaces merge together forming a weld.

Experimental studies and computational models have been reported on the underlying processes that drive solvent welding across polymers [21,33–36]. Two different frameworks have been used: case I or Fickian diffusion (obeying Fick’s law of diffusion) and case II or non-Fickian diffusion [36–41]. Case I applies in situations wherein polymer relaxation is fast and diffusion is the rate-limiting step. It is often observed in rubbery polymers. Case II applies when polymer relaxation is the rate-limiting step and is often observed in glassy polymers. As polymer chains start to rotate, interpenetration and entanglement of their branches across the interface join the two parts together. The joining process is thus regulated by a gradient in concentration of the solvent material and the softened polymeric material across the interface. This raises the question as to whether the scaling laws developed for the heat-mediated joining process above T_g are applicable to the chemistry-driven solvent-welding process. Second, does the assumption of modulus independence hold below strength evolution below T_g ? Third, do the time evolutions of strength (σ_{\max}), toughness (G_c), and stiffness (E) follow similar behavior?

The underlying bases for $t^{1/4}$ scaling of strength are that: (a) strength is directly proportional to the

^{*}Corresponding author: zubaer@udel.edu

stress-intensity factor; (b) following Irwin's formula, $K \propto \sqrt{G_c E}$, where K is the stress intensity factor, G_c is the critical energy release rate, and E is the elastic modulus; and (c) thermally activated movement of the polymer chains follows a subdiffusion process. These bases invoke three basic assumptions. First, Einstein's diffusion law, which states the mean-squared displacement is directly proportional to time:

$$\langle \Delta x^2(t) \rangle \propto t, \quad (1)$$

is applicable for the polymer joining process, where Δx denotes displacement of a monomer relative to the interface and t is time. Second, the number of polymer chains that cross the interface over time is proportional to the square root of the mean-squared displacement of the molecules of the solvent:

$$n(t) \propto ((\Delta x^2(t)))^{1/2}. \quad (2)$$

Third, the underlying process is independent of elastic modulus E , such that the time evolution of strength is fully controlled by the time evolution of the critical energy-release rate [11]:

$$\frac{\sigma}{\sigma_0} = \frac{K_I}{K_{I0}} = \sqrt{\left(\frac{G_c}{G_{c0}}\right)}, \quad (3)$$

where σ_0 , G_{c0} , and K_{I0} are material properties at $t = t_s$, which is the time beyond which no further change in properties occur at the interface. This relationship fits a number of experimental results conducted above T_g . However, one key limitation is that it overpredicts the long-time behavior of the evolution process. Also, it does not yield a constant value of strength over time. The onset of saturation is thus ill-defined in this model, and the time required to reach the saturated state is undefinable.

A fundamentally different but relevant physical process is dissolution [42], wherein a finite particle under a fully immersed condition gets completely swallowed by the solvent medium. At a constant temperature, the disintegration can be deemed to be a kinetic process [43,44]. For two solids bonded by a solvent (which is initially in the liquid state but later becomes a part of the solid bonded bilayer), it can be argued that both the diffusion and dissolution processes are closely related below T_g and driven by the gradient in the chemical potential across the evolving solvent-polymer interface. As the volume of the solvent solution is much higher compared to what is required to dissolve the polymers, the only choice for the solvent is to initiate the dissolution process locally, soften the molecular bonds of the polymer material, and help the monomer chains crosslink across the interface forming a solid phase. Dissolution is thus closely related to solvent welding. A scientific understanding of the role of dissolution is therefore highly desirable to construct the basis for the time evolution behavior of strength in solvent welding.

Focusing on the scaling laws of strength evolution and its correlation with dissolution, we employ a combination of diffusion and dissolution experiments and perform continuum scale simulations to unravel the determinants of interfacial strength. Our results show that the strength evolution follows a regular diffusion process, as opposed to the widely conjectured subdiffusion process. Additionally, results show that

strength evolution follows an exponential law and it represents both the evolution and saturation processes completely.

The paper is organized as follows. First, we describe the experimental procedure and findings on time evolution of interfacial strength. Second, we elaborate a computational approach to model the time evolution of strength and explore its determinants. Third, we explain experimental findings on the dissolution of polymer particles and its relationship with the polymer joining process.

II. SCALING LAWS OF STRENGTH EVOLUTION

A. Experimental approach

To investigate the time evolution of interfacial strength, we prepare samples by joining two identical poly(methyl methacrylate) (PMMA) polymer pieces together by a thin solvent layer. The samples are subject to uniaxial load applied normal to the interface at different curing times. The force-displacement data at each of the curing times are recorded and they are converted to the stress and strain data by using the cross-sectional area of the sample and its initial length. The strength of the interface at curing time t , denoted here as $\sigma_{\max}(t)$, is then calculated as the maximum stress of the stress-strain curve at t .

All samples are produced using a computer numerical controlled machining process to ensure dimensional accuracy. In the case of configurations with interfaces, bond surfaces of the constituent layers are prepared with a few additional steps. Bond surfaces are first sanded using 400-grit sandpapers and then are polished in the direction perpendicular to the thickness of the specimen using 1200-grit sandpapers. Finally, the surfaces are cleaned using a lint-free cloth soaked in isopropyl alcohol (rubbing alcohol) to remove any loose particles. All specimens in this study have 5.08 mm thickness.

For measuring the strength of the interface, we conduct tensile tests based on the ASTM standard D638-14 [45] established for strength testing of plastics. To measure interfacial strength, the dog-bone specimen of the tensile strength test is cut entirely in the middle and then bonded together to form an interface. Once bonded together, the sample has the exact same dimensions as the tensile strength test specimens. This is one of the several methods proposed by Krishnan and Xu [46] for tensile strength testing of adhesives in a layered homogeneous and bimaterial system. This method was adopted by Alam *et al.* [47] and Sundaram and Tippur [48], to measure interfacial strength in bilayer PMMA and glass systems, respectively. A rectangular frame with five properly shaped cutouts is used to place the cut pieces, add solvent, and press them together to form the desired interface. The polished surfaces are placed lightly together and the solvent (Weld-On 4) is applied to the edge of the joint with a syringe. After waiting a few seconds, the interface is then cured up to different duration to attain different interfacial conditions.

B. Results and discussion

The data points $[\sigma_{\max}(t), t]$ representing the time-evolution of interfacial strength are presented in Fig. 1. The results show that the interfacial strength increases exponentially with the curing time and approaches a constant value of

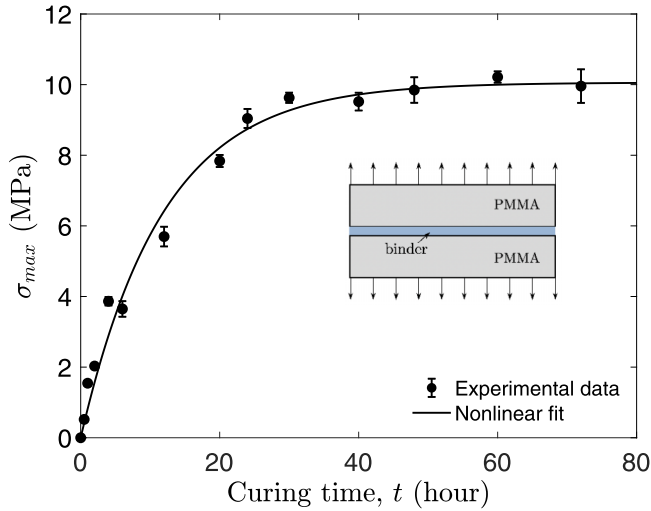


FIG. 1. Strength variation as a function of the curing time t . The schematic shows the sample configuration and loading direction applied for the uniaxial tensile tests. The data points (shown by the filled circles) are fitted by the exponential equation $\sigma_{\text{sat}}[1 - \exp(-\alpha t)]$, represented by the solid line. Here $\sigma_{\text{sat}} = 10.06$ MPa is the maximum possible interfacial strength and $\alpha = 0.08474$. The goodness of fit is measured as $R^2 = 0.9817$. The time required to achieve the saturated strength is around $t_c = 70$ h.

$\sigma_{\text{sat}} = 10.06$ MPa. The curing time required to reach this saturated state is denoted here as t_c . The t -dependent behavior of interfacial strength is well reflected by the following equation:

$$\sigma_{\text{max}}(t) = \sigma_{\text{sat}}(1 - e^{-\alpha t}), \quad (4)$$

where α is a fitting parameter describing the rate of strength evolution. The physical basis of this form is that $\sigma_{\text{max}}(t)$ should approach the maximum possible value σ_{sat} as $t \rightarrow \infty$. Regardless of the underlying processes responsible for bonding the PMMA materials, there must be a time t_c beyond which no further strengthening is possible. As the quantities t_c and σ_{sat} characterize a set of properties achieved by the binder material and the materials to be bonded, they are deemed to be interconnected for a material-solvent combination. We therefore describe the strength evolution process with a nondimensional quantity:

$$\frac{\sigma_{\text{max}}(t)}{\sigma_{\text{sat}}} = 1 - \exp\left(-\beta \frac{t}{t_c}\right) = 1 - \exp(-\beta t^*), \quad (5)$$

where $\beta = \alpha t_c = 6.35$ and the ratio $t^* = t/t_c$ is nondimensional time. The quantity β denotes how fast the interfacial strength reaches the maximum nondimensional strength. This nondimensional form indicates that all material properties that can affect the time evolution of strength are reflected by the single parameter β , which in turn depends on t_c . Thus, we postulate that Eq. (5) is applicable for any solvent-polymer joining process at temperatures below the glass-transition temperature such that the time-dependent behavior of the underlying molecular processes is independent of the material-solvent combination.

Furthermore, the exponential form is indicative of an Arrhenius type relationship, in which the exponent involves the ratio between an activation energy and a temperature-dependent factor. Here, we have that ratio between an instantaneous time and the time taken to reach the saturated strength. The underlying process is thus assumed to be a kinetic process as opposed to a thermodynamic process. The rate constant describing the kinetics of strength evolution is obtained as

$$\kappa = \frac{\sigma_{\text{sat}} - \sigma_{\text{max}}(t)}{\sigma_{\text{sat}}} = \exp\left(-\frac{\beta t}{t_c}\right). \quad (6)$$

It is important to note that this form captures the evolution of interfacial strength over the entire regime (covering the rapid change in strength in the evolution regime followed by a slower transition into the saturation regime). While temperature does not appear explicitly in this form, it is possible to apply this form at different temperatures by taking both β and σ_{sat} as a set of temperature-dependent material parameters.

In the literature, for a melting-driven joining process above the glass-transition temperature, the strength evolution has long been described to scale as $t^{1/4}$. The foundation of this scaling is the assumption that strength is proportional to the stress-intensity factor (K_I), the stress-intensity factor is proportional to the square-root of fracture toughness (G_c), the fracture toughness is proportional to the mean-squared displacement ($\langle \Delta x^2 \rangle^{1/2}$) of the monomers crossing the physical interface, and the mean-squared displacement varies as t . The scaling between interfacial strength and curing time is traditionally shown in a plot where the ordinate is the interfacial strength and the abscissa is $t^{1/4}$. This results in a linear line in the plot where the line passes through the origin, confirming that interfacial strength is zero at $t = 0$. This scaling is found to be followed by PMMA-PMMA, PMMA-SAN, and SAN-SAN polymer combinations, where SAN refers to styrene acrylonitrile [11]. Also, these plots show that the slope of the linear line increases with increasing the sample temperature above the glass-transition temperature. This prompts a question as to what extent the $t^{1/4}$ scaling in a solvent-welding process is applicable. We investigate this by plotting the data points $[\sigma_{\text{max}}(t), t]$ of Fig. 1 as $\sigma_{\text{max}}(t)$ vs $t^{1/n}$ plots for different choices of n in Fig. 2.

It is evident that, for each of the choices of n , the data points are well fitted by a linear line, and there is more than one value of n that can provide a linear relationship between σ_{max} and $t^{1/n}$. Secondly, the linear line provides the best fit curve when the data points up to the time $t = 30$ h are considered. We define this time as the “transition time” and denote it by t_t . It is important to note that the behavior of the regime $t_t \leq t \leq t_\infty$, which we call the “saturation regime,” is not captured by any of the power-law function. While the strength at $t = t_t$ is close to the highest interfacial strength, the power law does not describe the strength saturation regime. At $t = t_t$, the interfacial strength equals the maximum strength achievable from the polymer-solvent combination. In general, $t_c > t_t$ for the reason that the exponential approximation gives a smoother transition into the saturation regime and that at $t > t_t$ the exponential curve gives a smaller strength compared to the power laws.

Furthermore, unlike the melting-driven joining process, the line does not go through the origin for $n = 4$ or any of the

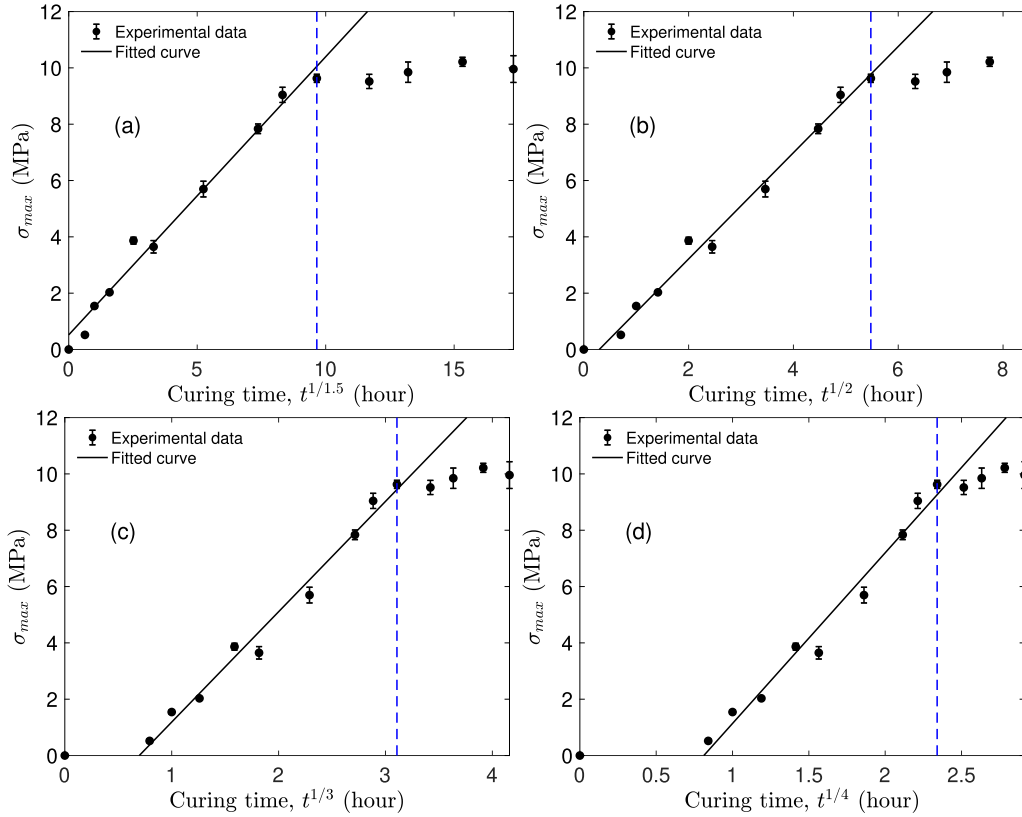


FIG. 2. Plots of the interfacial strength vs (a) $t^{1/1.5}$, (b) $t^{1/2}$, (c) $t^{1/3}$, and (d) $t^{1/4}$, where the unit of t is hour. The left side of the vertical blue line represents the time period over which the evolution of strength takes place and the right-hand side represents a steady state of interfacial strength. Fitting $\sigma = \alpha_1 + \alpha_2 t^{1/n}$ to the data points, the constants are obtained as $\alpha_1 = 0.52$, $\alpha_2 = 0.9875$ for $n = 1.5$; $\alpha_1 = -0.55$, $\alpha_2 = 1.886$ for $n = 2.0$; $\alpha_1 = -2.731$, $\alpha_2 = 3.981$ for $n = 3.0$; and $\alpha_1 = -4.921$, $\alpha_2 = 6.061$ for $n = 4.0$. Both α_1 and α_2 depend linearly on n : $\alpha_1 = 3.841 - 2.2n$ and $\alpha_2 = -2.136 + 2.04n$. The vertical dashed blue line represents the transition line at $t = t_t = 30$ h.

other three choices. Also, there are clearly two characteristic regimes in the linear relationship between σ_{\max} and $t^{1/n}$, regardless of the value of n . One regime describes the evolution of strength up to the maximum value of strength, and another is the continuation of the process into the saturation regime wherein strength reaches a steady state. The power-law scalings show the strength to continue to increase as t increases, thereby suggesting the transition into the saturation region to be poorly conceived by the power law. Furthermore, any relation of the form $\sigma_{\max} \propto t^{1/n}$ is valid only in the evolution regime. The choice of n is therefore not unique (as far as the linearity between σ_{\max} and $t^{1/n}$ is concerned), unless the condition $\sigma_{\max}(0) = 0$ is enforced in the fit. The closest we get to satisfy the condition with the best fit curve occurs for $n = 2$. This indicates that the evolution of strength scales as \sqrt{t} . Thus, the strength evolution at a constant temperature is a faster process than what is obtained for the melting-driven joining process. In Sec. III, from a continuum scale analysis, we show that the basis for this faster behavior is that the strength evolution depends on both toughness and stiffness.

Since the power laws describe the strength evolution reliably up to $t = t_t$ and the exponential fit describes both the evolution and saturation regimes reasonably well, we investigate the difference between these two approximations to understand the strength saturation process purely from a math-

ematical standpoint. In Fig. 3, we plot the experimental data along with the power law and the exponential fit. It is clear that any equation of the form $t^{1/n}$ can be assumed to accurately represent the experimental data points, at least visually; but none of them represents the behavior of the data points at $t > t_t$. To determine the degree of nonlinearity that governs the difference between the exponential and power-law approximations, we expand the exponential function as follows:

$$\sigma_{\max}(t) = \sigma_{\text{saturated}} \left(\beta t/t_c - \frac{(\beta t/t_c)^2}{2!} + \frac{(\beta t/t_c)^3}{3!} - \dots \right)$$

and plot it with different terms from its expansion. We find that the series expansion should have at least up to the seventh order term, $\frac{(\beta t/t_c)^7}{7!}$, to correctly represent the behavior of the time-evolution process. The even-order terms represent a reduction in strength while the odd-order terms represent an increase in strength. Their linear combination is needed to correctly capture the time-evolution behavior over the entire strength evolution and saturation regimes. However, to capture the behavior of the saturation regime, we need the complete expansion of the exponential function. On the contrary, a power-law approximation always overestimates strength in the saturation regime, because $t^{1/n} \rightarrow \infty$ as $t \rightarrow \infty$ for any value of n .

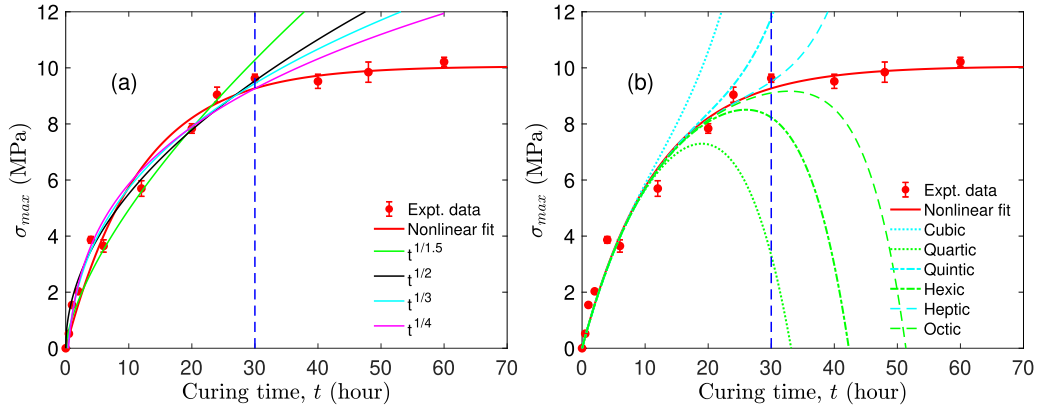


FIG. 3. Left: Strength variation as a function of the curing time t . The data points (shown by filled circles) are fitted by the nonlinear equation: $\sigma_{\max}[1 - \exp(-\alpha t)]$ where the fitting parameters are $\sigma_{\max} = 10.06$ MPa and $\alpha = 0.08474$ with a goodness of fit measured as $R^2 = 0.9817$. Best-fit curves of the form $\sigma_{\max} = \alpha_1 + \alpha_2 t^{1/n}$ for different choices of n are shown by the solid lines. The values of α_1 and α_2 are available in Fig. 2. Right: Comparison of the series expansion of the exponential function with a truncation of order $O(t^n)$. The vertical dashed blue line represents the transition line at $t = t_t = 30$ h.

The difference between the power-law and exponential scalings, denoted here by R , can be written as

$$R = \int_0^{t_t} (\sigma^{\text{exponential}} - \sigma^{\text{power}}) dt. \quad (7)$$

$$R = \int_0^{t_t} \left\{ \sigma_{\text{saturated}} \left[1 - \exp\left(-\frac{\beta t}{t_c}\right) \right] - [c_1 + c_2 n + (c_3 + c_4 n)t^{1/n}] \right\} dt \quad (8)$$

$$= \sigma_{\text{saturated}} \left(t_t + \frac{t_c \exp(-t_t \beta / t_c) - t_c}{\beta} \right) - (c_1 + c_2 n)t_t - (c_3 + c_4 n) \frac{nt_t^{(1+n)/n}}{n+1}. \quad (9)$$

Substituting the values of $c_1 = 3.841$, $c_2 = -2.2$, $c_3 = -2.136$, $c_4 = 2.04$, $t_t = 30$ h, $t_c = 70$ h, $\beta = 6.35$, and $\sigma_{\text{saturated}} = 10.06$ MPa, the residual is found to have a minimum at $n = 2.35$. However, the linear line $\sigma_{\text{saturated}}$ vs $t^{1/2.35}$ does not go through the origin. The linear fit of the data points in the range $0 \leq t \leq t_t$ goes through the origin when $n = 1.74$. As a result, if we are to find an optimum value of n ensuring $\sigma_{\max}(0) = 0$ and making the residual as close to the minimum as possible, we get $n = (2.35 + 1.74)/2 = 2.045 \approx 2.0$. From this, we conclude that the interfacial strength in the solvent-welding process scales as \sqrt{t} . This behavior differs from what was reported back in 1981 [11] on tests in a melting-driven joining process above the glass-transition temperature.

One could argue that the discrepancy may arise from different experimental and sample conditions: in the previous study an initial crack was present and the joining process was thermally driven, whereas this study is conducted at room temperature and without the presence of an initial crack. It should be noted that, in all of our stress-strain tests, the stress-strain behavior is linear. Even if we consider an initial crack present at the interface, we will still get the same $\sigma_{\text{saturated}}$ vs \sqrt{t} relation. The $t^{1/4}$ type scaling was built on the approximation that strength is proportional to the square-root of the interfacial toughness G_c only and independent of E . We therefore question the validity of the assumption that

Minimizing the residual with respect to the exponent n , we explore a value of n that offers the best power-law fit in the regime: $0 \leq t \leq t_t$. Using the series expansion, we get a closed-form expression for R :

$K_I/K_{I_0} = G_c/G_{c_0}$, where K_{I_0} and G_{c_0} are the stress-intensity factor and the critical energy release rate at the reference state (at $t = t_\infty$). If G_c follows a regular diffusion process and modulus is assumed to be a constant, strength is obtained as a subdiffusion process. This contradicts our experimental findings and the R -based discussions outlined above. Our finding of strength evolution as a $t^{1/2}$ process highlights an important point that strength evolution is a regular diffusion process, similar to the evolution of interfacial toughness.

If we are to assume G_c to depend on the width of the diffusive regime, G_c scales as $t^{1/2}$, as originally proposed in Ref. [11]. The modulus dependence of Irwin's formula would suggest that it should evolve as $t^{1/2}$ for the strength to scale as $t^{1/2}$. The scaling of modulus was not taken into consideration in determining the original scaling law for strength evolution in melting-driven joining processes. Thus, to be consistent with the linear elasticity relation that $\sigma \propto \sqrt{G_c E}$, stiffness should also follow a regular diffusion process, as opposed to being a constant. As strength is an effective property for the bonded polymer at a given time, its determinants G_c and E can vary spatially across the interface. It is important to explore what type of scaling toughness and stiffness follow to form the physical foundation for strength of the entire domain. This is a nontrivial experimental task due to the difficulty in determining the local variations of G_c and E at different points along the interface at different curing times. As an

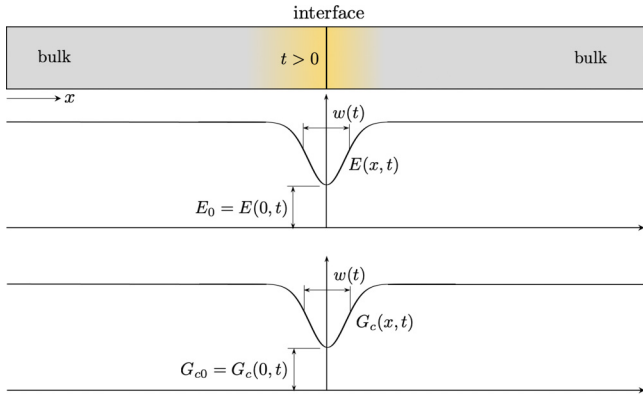


FIG. 4. Schematic of the joined polymers with the yellow color representing a state during diffusion of the solvent material. Two spatially varying profiles of $E(x)$ and $G_c(x)$ with their minimum showing at the interface. Over time the minimum increases and ultimately reaches the bulk value giving the maximum strength and toughness for the joint.

alternative, we employ a continuum scale analysis as described next.

III. DETERMINANTS OF STRENGTH EVOLUTION

A. Computational approach

To model the time-evolution of strength, we construct a continuum domain with two parts acting as the bulk polymer joined by an interface region with its properties varying spatially normal to the interface. Assuming the time-dependent properties to be directly dependent on the density of the solvent monomer, we consider a normal distribution for the concentration of the polymer chains. Following the solution to the thin-film diffusion equation in one dimension [49–51], we get

$$N(x) = \frac{1}{\sqrt{4Dt\pi}} \exp\left[-\frac{(x - x_{\text{interface}})^2}{4Dt}\right] \quad (10)$$

$$= \sqrt{\frac{1}{\beta\pi}} \exp\left[-\frac{(x - x_{\text{interface}})^2}{\beta}\right], \quad (11)$$

where $N(x)$ is the concentration at x and $\beta = 4Dt$ is the half width at half maximum (HWHM). Assuming the mean-squared displacement to be directly proportional to the curing time, $\langle(x(t) - x(0))^2\rangle \propto t$, it can be seen that $\beta \propto t$. The quantity $1/\beta$ characterizes the speed of the diffusion process and scales its intensity. The time evolution of $N(x)$ can thus be described by the time evolution of the intensity and speed through the parameter β . The intensity varies as t and the speed varies as $t^{1/2}$. Therefore, the evolution of strength can be modeled in quasistatic finite element simulations using a domain with an interface and varying its properties under the approximation that localized properties at the interface are directly proportional to $N(x)$. The spatial variation of $G_c(x)$ and $E(x)$ at an arbitrary time $t > 0$, is shown schematically in Fig. 4. The mechanical properties that describe the local criterion for strength depends on the pointwise Young's modulus (E) and toughness (G_c). Both E and G_c are directly related

to the average cross-linking density of the solvent monomers across the interface, thereby, the normal distribution of the monomers and the HWHM.

For modeling deformation, we employ continuum scale simulations using the variational phase-field modeling of fracture [52,53] with elemental properties varying along the loading direction. In this framework, the total energy of a linearly elastic domain is written as a sum over the elastic energy and the surface energy [54,55]:

$$W = \int_{\Omega} \frac{1 - v^2}{2} e(u) : C : e(u) + \frac{3G_c}{8} \left(\frac{v}{l} + l|\nabla v|^2 \right) dA,$$

where W is the total energy, $:$ denotes a tensor product, v is the damage variable, $e(u)$ is the strain due to displacement field u , G_c is the pointwise critical energy release rate, C is the pointwise elastic modulus, and l is an internal length. The first term describes the elastic energy and the second term the surface energy. The intact phase is represented by the first term for $v = 0$, while the fractured phase by the second term for $v = 1$. The interphase is represented by a combination of the terms with $0 < v < 1$ representing a transition from the intact phase to the surface.

The internal length l determines the width of the fracture regime. The localized stress required to create nucleation of cracks in this model is defined as [56]

$$\sigma_c = \sqrt{\frac{3G_c E}{8l}}. \quad (12)$$

It should be noted that σ_c is a local property satisfied by the finite element solution in minimizing the energy at the neighborhood of the element undergoing a phase-change from an intact state to a fractured state. It does not reflect the longer scale elemental features that may involve multiple elements, describing the macroscopic or effective state of the domain. As such, σ_c refers to a local elemental property, as opposed to a macroscopic property of the domain. The implicit integration enables assigning pointwise material properties to the elements.

To model the spatially varying continuous properties of the elements via $E(x)$ and $G_c(x)$, we use a python script to create and group the elements normal to the loading or x direction in 42 strips, where there are 41 strips (each of width 0.2) representing the interface regime and the remaining strip is of width 21.8 representing the bulk domain. Here, the length scales and the material properties are nondimensionalized following [54]. The first group is the elements normal to the interface following the profiles denoted by Eq. (13). They form vertical strips with a collection of elements. The width of each of the vertical strips forming the interface regime is taken as $h = 0.2$. Thus, the width of the fracture surface is on the order of h . This ensures that the fracture width is larger than the strip width. Also, the element size is taken as $h = 0.1$, which is sufficiently small for the results to converge with respect to the mesh size. Strength of the domain is calculated by determining the fracture strain from the elastic energy vs strain plots and multiplying it by the effective elastic modulus obtained from the stress-strain curve.

B. Results and discussions

To determine the individual role of $G_c(x)$ and $E(x)$, we consider three cases: (i) E is homogeneous but G_c varies spatially:

$$G_c(x) = \frac{1}{\sqrt{\beta\pi}} \exp\left[-\frac{(x - x_{\text{interface}})^2}{\beta}\right],$$

$$E(x) = E;$$

(ii) G_c is homogeneous but E varies spatially:

$$E(x) = \frac{1}{\sqrt{\beta\pi}} \exp\left[-\frac{(x - x_{\text{interface}})^2}{\beta}\right],$$

$$G_c(x) = G_c;$$

and (iii) both E and G_c vary spatially:

$$E(x) = G_c(x) = \frac{1}{\sqrt{\beta\pi}} \exp\left[-\frac{(x - x_{\text{interface}})^2}{\beta}\right]. \quad (13)$$

Here, the parameter $\beta \propto t^n$, and the exponent n prescribes whether the underlying molecular mechanism is a subdiffusion ($n < 1$), diffusion ($n = 1$), or superdiffusion ($n > 1$) process. In modeling the behavior of the domain with spatially varying $G_c(x)$ and $E(x)$ properties at a given t , the profiles are normalized with the respective values of the bulk, representing the properties of the material far from the interface. Taking $n = 1$, we construct different profiles of $G_c(x)$ and $E(x)$ for different choices of t . We then conduct tensile tests to determine $\sigma_{\text{max}}(t)$ using the finite element method (FEM) simulations, under the assumption of linear elasticity. We find that only the condition wherein both E and G_c follow a Gaussian distribution results in a commensurate variation in the effective strength of the domain. Plotting the $\sigma_{\text{max}}(t)$ vs t data points for case (iii), we find the strength to scale as $t^{0.42}$, which is close to the experimentally obtained scaling of $t^{0.5}$, as illustrated in Fig. 5.

While the local variation in stiffness at the interface does not affect the effective stiffness of the bilayer, it affects the criteria for initiating failure at the interface for the reason that failure requires reaching a critical value. Regardless of the site, a critical stress state can trigger failure in the bilayer. Thus, the strength of the interface must depend on the location variation in stiffness as well as toughness, as prescribed by the linear elasticity relation that $\sigma \propto \sqrt{G_c E}$. It can be asserted that both $G_c(x, t)$ and $E(x, t)$ scale as \sqrt{t} such that the time evolution of strength follows a \sqrt{t} type behavior:

$$\begin{aligned} \sigma_{\text{max}}(t) &\propto \sqrt{G_c(t)E(t)} \\ &\propto \sqrt{(t^{1/2})(t^{1/2})} \\ &\propto \sqrt{t}. \end{aligned}$$

As the pointwise toughness and modulus are both the minimum at $x = 0$, the strength of the bilayer is determined by the local strength of the interface at $x = 0$. Thus, our continuum scale model also supports our assertion that both the modulus and fracture toughness scale as \sqrt{t} . And the combined effect of \sqrt{t} behavior of stiffness and fracture toughness is that strength also varies as \sqrt{t} . We therefore conclude that the effective interfacial strength, toughness, and stiffness vary as \sqrt{t} , highlighting the evolution of each of these material

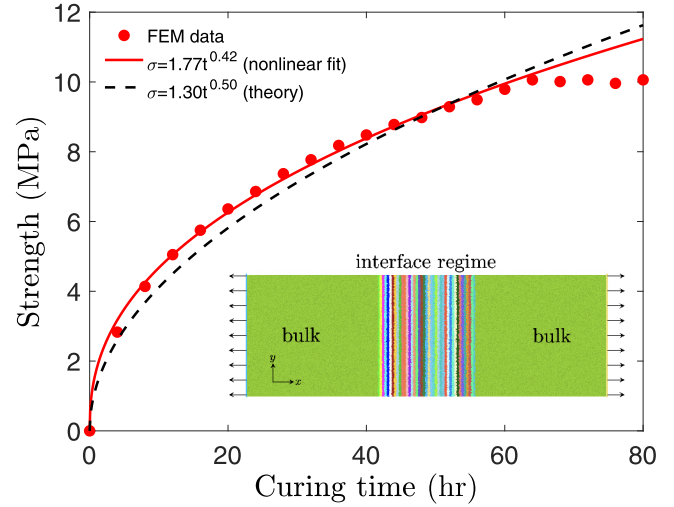


FIG. 5. Interfacial strength for different profiles of $E(x, t)$ and $G_c(x, t)$ for a given choice of t , parametrized by β . Each data point represents the critical stress (or strength) at which the interface failed for a selected profile of $E(x, t)$ and $G_c(x, t)$. The variation in strength for each choice of the exponent n is fitted by a nonlinear equation of the form $c_1 t^n$. The inset shows the finite element domain with 41 strips at the interface regime. The domain is loaded along the x direction and its stress-strain responses for different profiles are examined, as described in the text. The properties $G_c(x, t)$ and $E(x, t)$ of the strips follow the mathematical profiles described in the text.

properties as a regular diffusion process. This supports the experimental results and sheds light on how strength evolves over time in a solvent-welding process. Our finding contradicts the previous assertion that strength scales as $t^{1/4}$. It underscores the importance of taking into account stiffness variation in the dimensional analysis of strength.

In the next section, we investigate the dissolution process of polymer macroparticles in order to establish a connection between dissolution and joining in the context of solvent-mediated welding of polymers. We show that there is a direct point-to-point connection between these two processes, and dissolution experiments can offer an easy route for determining the time-dependent interfacial strength in solvent welding of polymers.

IV. SCALING LAWS OF DISSOLUTION AND SOLVENT WELDING

In dissolution, the volume of the solid material is much less than that of the solvent, and over time the entire solid material is dissolved in the solvent. The underlying mechanisms involve propagation of a solid-liquid interface driven by a concentration gradient across the interface. On the other hand, in the joining process, the solvent dissolves the solid material at the interface, but, due to the finite volume of the solvent, the solid undergoes a softening process as opposed to complete disintegration into the solvent. Dissolution can thus be assumed to be an inverse of the joining process with respect to the relative change in the volume of the material phase of the interacting materials. With an objective of understanding the parameter β , which characterizes the evolution of strength,

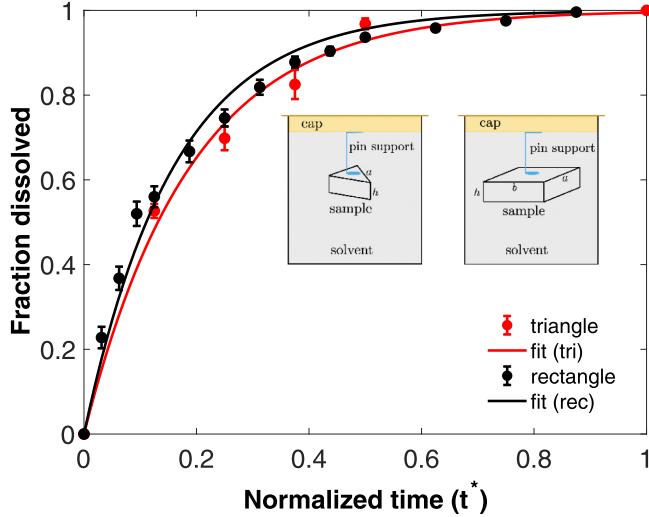


FIG. 6. Experimental data on the fraction dissolved of the PMMA sample as a function of the normalized curing time, for particles of two different shapes. Fitting $1 - \exp(-\beta t^*)$, we get $\beta = 5.281890$ for triangle and $\beta = 6.2572$ for rectangle, where $t_c = 2$ h for the triangle and $t_c = 8$ h for the rectangle. The surface-to-volume ratio is $(2\sqrt{3}a^2/4 + 3ah)/(h\sqrt{3}a^2/4) = 1.51$ for the triangle; and $2(ab + bh + ah)/(abh) = 0.63$ for the rectangle, indicating the surface-to-volume ratio for the triangular sample to be 2.39 times higher than the rectangular sample. The pin support shown in the schematic drawn in the inset is to make sure the PMMA sample continues to be immersed throughout the entire dissolution process.

here we conduct separate sets of experiments with a piece of PMMA material immersed in a bath of the Weld-On 4 solvent. We determine (i) how long it takes for the samples of different geometric parameters to completely dissolve in the Weld-On 4 solution and (ii) what geometry-related features (such as surface and volume) dominate the rate of dissolution in the solution.

We consider two PMMA samples with very different shapes: one has an equilateral triangular cross section with side length a and height h , and the other has a rectangular cross section of side lengths a and b and height h . Both samples have $h = 5.08$ mm, while the triangular sample has $a = 6.21$ mm and the rectangular has $a = 65$ mm and $b = 10$ mm. We have immersed them in separate test tubes filled with Weld-On 4. Recovering the samples from the test tubes at different curing times for each shape, we measure the weight loss of the samples and plot the “fraction dissolved” or weight loss, denoted as χ , as a function of the normalized time t/t_c , where t_c is the time taken by the sample to fully dissolve in the solvent. The time-dependent behavior of χ is shown in Fig. 6.

Results show that the normalized time-dependent behavior of χ is shape independent. Also, the dissolution behavior of χ follows (the same mathematical form that we used in describing the evolution of strength):

$$\chi = 1 - \exp(-\beta t^*), \quad (14)$$

where t^* is the normalized curing time describing the ratio between the total instantaneous time and the total time required for completing dissolution. The values of the parameter

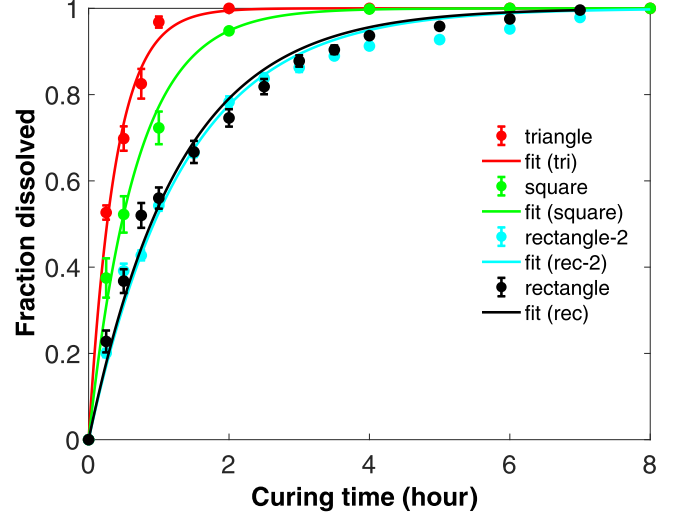


FIG. 7. Experimental data on the fraction dissolved of the PMMA sample as a function of the curing time t , for particles of three different shapes and four different sizes. Fitting $1 - \exp(-\alpha t)$, we get $\alpha = 2.641$, 1.479 , 0.747 , and 0.747 for the triangle, square, and the rectangular shapes, respectively.

are $\beta = 5.281$ for the triangular shaped sample and 6.257 for the rectangular shaped sample. They are within a small percentage of the parameter β used in Eq. (5). Dissolution and interfacial strength are thus linearly correlated:

$$\chi = \frac{\sigma}{\sigma_{\max}} \quad \forall t^*. \quad (15)$$

At a given normalized curing time t^* , it is therefore possible to know the strength of a curing process without doing destructive tensile tests. For example, if the maximum interfacial strength $\sigma_{\text{saturated}}$ and the required curing time t_c are known for a solvent-matrix combination, we can determine the interfacial strength at any arbitrary curing time upon determining the parameter β from a simple dissolution test.

The observations lead to an important finding: the time evolution of strength or fraction dissolved is strongly dependent on the parameter t_c , which is different across the different samples used in the dissolution tests and the tensile tests. To examine the behavior of t_c , we determine the “fraction dissolved” vs “curing time” behavior for a second rectangular sample of different dimension than the first sample and for a sample with square cross section. As shown in Fig. 7, the dissolution curves exhibit a clear dependence on the sample shape. The dissimilarity between the square, triangular, and rectangular samples and a close similarity between the rectangular samples of very different dimensions highlight an important shape effect in the dissolution process. The large difference between the values of t_c for the strength evolution and dissolution of the particles can be attributed to the role of dimensionality. For the dissolution of the particles, the reaction process is three-dimensional as the particles are completely immersed in the solvent and the concentration gradient at the interface between the solvent and particle can be assumed to remain at the same level throughout the dissolution process. On the other hand, for the strength evolution process, the solvent amount is finite and its reaction with

the PMMA is one-dimensional in nature where the solvent interaction with PMMA is normal to the interface. It can thus be concluded that dissolution and joining processes are closely related. Nonetheless, when plotted against t^* , all of these curves overlap.

As the rectangular samples show similar behavior in spite of a difference in their volume, we propose that it is the surface-to-volume ratio that describes the shape-dependent dissolution process. For the samples considered above, the surface-to-volume ratios are 1.51 (triangle), 0.87 (square), and 0.63 (rectangle). The values of α are 2.641, 1.479, and 0.747, respectively, and the values of t_c are 2, 4, and 8 h, respectively. The variation of α is linearly related to the surface-to-volume ratio. The larger the ratio the smaller the curing completion time. This is an important finding in the sense that from a few simple dissolution tests on simpler shapes (square), it is possible to extract the behavior for complex geometric shapes (such as dodecahedrons). Similarly, regardless of the complexity in the geometric shapes, it is possible to predict the strength evolution behavior for a binder-matrix combination.

To extract a theoretical basis behind the t_c -dependent behavior of dissolution and the interfacial strength, we make a hypothesis that this quantity is proportional to the surface-to-volume ratio:

$$t_c \propto S/V = \gamma S/V, \quad (16)$$

where S and V are the total surface area exposed to the solvent and the volume dissolved, respectively, and γ is the proportionality parameter (which needs to be evaluated once for a given binder-matrix combination). Its unit is h-mm. In terms of these parameters we can write the ratio χ as

$$\chi = \frac{\sigma}{\sigma_{\max}} = 1 - \exp\left(-\beta \frac{tV}{\gamma S}\right). \quad (17)$$

It should be noted that for a dissolution experiment with finite particles, both S and V are known quantities. For two semi-infinite plates, S can be assumed to be equal to the surface area exposed at the bonded interface, but the volume that participates during the dissolution process is unknown. Using the relation and known properties, it is, however, possible to determine how much volume of the bonded materials is used up during the binding process, without conducting any nanoscale expensive and time-consuming experiments. From our dissolution tests on the samples of height h and length L , the parameter $\gamma \approx 3/2$ h-mm. Thus, $t_c = \gamma S/V = \gamma(Lh)/(Lh\delta) = \gamma/\delta$ yields the depth of dissolution during the binding (or strength evolution) process as $\delta = \gamma/t_c = 21.4 \mu\text{m}$, where $t_c = 70$ h.

The similarity between the joining process below T_g and dissolution hints at a possible one-to-one correspondence between interfacial strength and the fraction of the bonded materials dissolved during the joining process. The higher

the dissolution, the higher the strength. Consequently, the exponent β appearing in the expressions of strength and fraction dissolved can be determined from either the tensile tests or the dissolution tests. It highlights an important point that it is sufficient to conduct dissolution experiments to predict the strength evolution of a combination of materials and solvents. The analysis above is constructed with the assumption that there is a sufficient volume of the solvent available to completely dissolve the PMMA sample.

V. CONCLUDING REMARKS

The main conclusion of this work is that the evolutions of localized strength, toughness, and stiffness follow the same scaling law when the process occurs below the glass-transition temperature. This finding advances our understanding of the time-evolution of strength between two identical polymers subjected to a physical contact via a solvent below the glass-transition temperature. Both experimental and simulation results show that the underlying kinetics governing the strength evolution of interface is a purely diffusive and Gaussian process, and it scales as \sqrt{t} . Also, strength evolution is found to be directly related to the evolution of toughness and modulus, each of which also scales as \sqrt{t} . They are describable by the mean-square displacement of the polymer materials crossing the interface that has a linear dependence on time. Thus simple diffusion-based models are applicable to describe the evolution of interfacial strength. Although the widely known $t^{1/4}$ behavior can capture strength evolution in the initial stage of the joining process, they overpredict the role of diffusion at longer timescales.

Furthermore, it is found that time evolution of strength is better represented by exponential functions. They not only capture the evolution behavior but also the saturation of strength at longer times. Simple power-law type scaling overestimates the strength at longer curing times. The entire history of strength, toughness, or stiffness evolution can thus be described as a kinetic process, and the details of the kinetics are closely captured by Einstein's diffusion model.

In addition to providing an understanding of the evolution of strength, toughness, and stiffness, we demonstrate that the joining process has a close equivalency to the dissolution process. A simple series of experiments on the dissolution of polymer particles reveals that dissolution tests can provide useful information on strength during the evolution process. The dissolution tests on different shapes show that the time-dependent behavior is closely described by the surface-to-volume ratio. The higher the ratio, the faster is the dissolution of the polymeric material into the solvent. These results are expected to offer new insights on the physics of the solvent-welded polymer joining process and find applications in polymer-based composites.

- [1] S. Amancio-Filho and J. Dos Santos, *J. Polym. Eng.* **49**, 1461 (2009).
 [2] V. K. Stokes, *Polym. Eng. Sci.* **29**, 1310 (1989).

- [3] A. Yousefpour, M. Hojjati, and J.-P. Immarigeon, *J. Thermoplast. Compos. Mater.* **17**, 303 (2004).
 [4] D. Y. Wu, S. Meure, and D. Solomon, *Prog. Polym. Sci.* **33**, 479 (2008).

- [5] R. R. Mishra and A. K. Sharma, *Composites, Part A* **81**, 78 (2016).
- [6] D. Stavrov and H. Bersee, *Composites, Part A* **36**, 39 (2005).
- [7] T. Ahmed, D. Stavrov, H. Bersee, and A. Beukers, *Composites, Part A* **37**, 1638 (2006).
- [8] U. Vaidya and K. Chawla, *Int. Mater. Rev.* **53**, 185 (2008).
- [9] M. J. Troughton, *Handbook of Plastics Joining: A Practical Guide* (William Andrew, Norwich, NY, 2008).
- [10] P.-G. de Gennes, *J. Chem. Phys.* **55**, 572 (1971).
- [11] K. Jud, H. Kausch, and J. Williams, *J. Mater. Sci.* **16**, 204 (1981).
- [12] X. Chen, M. A. Dam, K. Ono, A. Mal, H. Shen, S. R. Nutt, K. Sheran, and F. Wudl, *Science* **295**, 1698 (2002).
- [13] J. Klein and B. Briscoe, *Proc. R. Soc. London, Ser. A* **365**, 53 (1979).
- [14] K. Jud and H. Kausch, *Polym. Bull.* **1**, 697 (1979).
- [15] C. Bucknall, I. Drinkwater, and G. Smith, *Polym. Eng. Sci.* **20**, 432 (1980).
- [16] F. P. Price, P. T. Gilmore, E. L. Thomas, and R. L. Laurence, *J. Polym. Sci.: Polym. Symposia* **63**, 33 (1978).
- [17] F. Bueche, W. Cashin, and P. Debye, *J. Chem. Phys.* **20**, 1956 (1952).
- [18] S. J. Whitlow and R. P. Wool, *Macromolecules* **24**, 5926 (1991).
- [19] G. Reyes, M. Borghei, A. W. King, J. Lahti, and O. J. Rojas, *Biomacromolecules* **20**, 502 (2018).
- [20] A. Pizzi and K. L. Mittal, *Handbook of Adhesive Technology* (CRC, Boca Raton, FL, 2017).
- [21] Q. Shi, K. Yu, M. L. Dunn, T. Wang, and H. J. Qi, *Macromolecules* **49**, 5527 (2016).
- [22] R. D. Adams, J. Comyn, and W. C. Wake, *Structural Adhesive Joints in Engineering* (Springer Science & Business Media, New York, 1997).
- [23] M. Chanda, *Plastics Technology Handbook* (CRC, Boca Raton, FL, 2017).
- [24] R. Groele, P. Krasicky, S.-W. Chun, J. Sullivan, and F. Rodriguez, *J. Appl. Polym. Sci.* **42**, 3 (1991).
- [25] D. A. Edwards and D. S. Cohen, *AIChE J.* **41**, 2345 (1995).
- [26] E. J. Kappert, M. J. Raaijmakers, K. Tempelman, F. P. Cuperus, W. Ogieglo, and N. E. Benes, *J. Membr. Sci.* **569**, 177 (2019).
- [27] Ö. Pekcan, Ş. Uğur, and Y. Yılmaz, *Polymer* **38**, 2183 (1997).
- [28] S. M. Lee, J. H. Lee, and Y. C. Bae, *Fluid Phase Equilib.* **382**, 107 (2014).
- [29] J. Papanu, D. Hess, D. Soane, and A. Bell, *J. Appl. Polym. Sci.* **39**, 803 (1990).
- [30] X. Kuang, Q. Shi, Y. Zhou, Z. Zhao, T. Wang, and H. J. Qi, *RSC Adv.* **8**, 1493 (2018).
- [31] Y. Sun, H. Yang, W. Xia, and Y. Guo, *Appl. Surf. Sci.* **527**, 146947 (2020).
- [32] C. M. Hamel, X. Kuang, K. Chen, and H. J. Qi, *Macromolecules* **52**, 3636 (2019).
- [33] C. Lin, S. Lee, and K. Liu, *J. Adhes.* **34**, 221 (1991).
- [34] Q. Meng, *Mech. Mater.* **148**, 103516 (2020).
- [35] K. Haire, T. Carver, and A. Windle, *Comput. Theor. Polym. Sci.* **11**, 17 (2001).
- [36] R. P. Wool, B.-L. Yuan, and O. McGarel, *Polym. Eng. Sci.* **29**, 1340 (1989).
- [37] J. Papanu, D. Hess, D. Soane, and A. Bell, *J. Electrochem. Soc.* **136**, 3077 (1989).
- [38] L. Baij, J. J. Hermans, K. Keune, and P. D. Iedema, *Macromolecules* **51**, 7134 (2018).
- [39] J. Papanu, D. Soane, A. Bell, and D. Hess, *J. Appl. Polym. Sci.* **38**, 859 (1989).
- [40] G. R. Davidson III and N. A. Peppas, *J. Controlled Release* **3**, 243 (1986).
- [41] N. A. Peppas and N. M. Franson, *J. Polym. Sci., Polym. Phys. Ed.* **21**, 983 (1983).
- [42] B. A. Miller-Chou and J. L. Koenig, *Prog. Polym. Sci.* **28**, 1223 (2003).
- [43] F. Baletto and R. Ferrando, *Rev. Mod. Phys.* **77**, 371 (2005).
- [44] Y. Wang, J. He, C. Liu, W. H. Chong, and H. Chen, *Angew. Chem., Int. Ed.* **54**, 2022 (2015).
- [45] ASTM Standard, <https://www.astm.org/Standards/D638>.
- [46] A. Krishnan and L. R. Xu, *J. Adhes.* **87**, 53 (2011).
- [47] M. Alam, J. P. Parmigiani, and J. J. Kruzic, *Eng. Fract. Mech.* **181**, 116 (2017).
- [48] B. M. Sundaram and H. V. Tippur, *J. Mech. Phys. Solids* **96**, 312 (2016).
- [49] J. Crank, *The Mathematics of Diffusion* (Oxford University Press, New York, 1979).
- [50] E. L. Cussler and E. L. Cussler, *Diffusion: Mass Transfer in Fluid Systems* (Cambridge University Press, Cambridge, UK, 2009).
- [51] H. Li, Z. Wu, J. Yin, and J. Zhao, *Nonlinear Diffusion Equations* (World Scientific, Singapore, 2001).
- [52] G. A. Francfort and J.-J. Marigo, *J. Mech. Phys. Solids* **46**, 1319 (1998).
- [53] B. Bourdin, G. A. Francfort, and J.-J. Marigo, *J. Elast.* **91**, 5 (2008).
- [54] M. Hossain, C.-J. Hsueh, B. Bourdin, and K. Bhattacharya, *J. Mech. Phys. Solids* **71**, 15 (2014).
- [55] C. Hsueh, L. Avellar, B. Bourdin, G. Ravichandran, and K. Bhattacharya, *J. Mech. Phys. Solids* **120**, 68 (2018).
- [56] E. Tanné, T. Li, B. Bourdin, J.-J. Marigo, and C. Maurini, *J. Mech. Phys. Solids* **110**, 80 (2018).